# Numerical simulation of a Hypothetical Core Disruptive Accident in the MARA8 mock-up with the CASTEM-PLEXUS computer code

Marie-France Robbe, Yves Cariou, Michel Lepareux, Eloi Treille

# NUMERICAL SIMULATION OF A HYPOTHETICAL CORE DISRUPTIVE ACCIDENT IN THE MARA8 MOCK-UP WITH THE CASTEM-PLEXUS COMPUTER CODE

M.F. Robbe
*CEA Saclay, DRN-DMT-SEMT, 91191 Gif sur Yvette cedex, France*
*Tel: (33) 1 69 08 87 49, Fax: (33) 1 69 08 52 42, E-mail: mfrobbe@cea.fr*

Y. Cariou
*Novatome, NVPM, 10 rue Juliette Récamier, 69006 Lyon, France*

M. Lepareux
*CEA Saclay, DRN-DMT-SEMT, 91191 Gif sur Yvette cedex, France*

E. Treille
*Socotec Industrie, 1 av. du Parc, 78180 Montigny le Bretonneux, France*

**Abstract**

In case of a Hypothetical Core Disruptive Accident (HCDA) in a Liquid Metal Reactor, the interaction between fuel and liquid sodium creates a high pressure gas bubble in the core. The violent expansion of this bubble loads the vessel and the internal structures, whose deformation is important. The experimental test MARA8 is a simple small scale representation of a reactor. It simulates a HCDA in a mock-up closed by a flexible vessel and a flexible roof. The vessel is filled with water, topped with an air blanket. The test is fired using an explosive charge.

This paper presents a simulation of the MARA8 test with the fast dynamics code CASTEM-PLEXUS. A specific HCDA constitutive law was implemented in this code to simulate this kind of explosion. The computed results are explained by means of an analysis of the pressure, gas fraction, fluid velocities, displacements, strains and stresses.

## 1 INTRODUCTION

In case of a Hypothetical Core Disruptive Accident (HCDA) in a Liquid Metal Reactor, the interaction between fuel and liquid sodium creates a high pressure gas bubble in the core. The violent expansion of this bubble loads the vessel and the internal structures, whose deformation is important.

During the 70s and 80s, the LMFBR integrity was studied through several experimental programmes undertaken by several countries and by developing computer codes especially devoted to the analysis of transient loads resulting from a HCDA. The codes generally aimed at simulating a HCDA at reactor scale in order to demonstrate the capacity of the reactor to resist to such an accident. The experimental programmes had more varied objectives. For instance, the purpose of the FTR and CBR detail scale model [1] was to demonstrate that the Clinch River Breeder Reactor could withstand HCDA loads for licensing the reactor.

The STROVA and COVA programmes were dedicated to the validation of the computer codes. The STROVA programme [2] consisted in applying well defined transient loadings to a variety of metal structures (representative of the reactor roof and reactor vessel components) and to compare the experimental results with those computed by the structural dynamics code EURDYN.

The COVA programme [3,4,5] (COde VAlidation) relied on a series of experiments performed in cylindrical tanks, starting with simple tests and increasing in complexity in such a way that only one new feature was introduced at a time. This programme [6,7] aimed at validating the codes ASTARTE and SEURBNUK.

The WINCON and MARA programmes involved tests of gradual complexity which were based on small scale replicas of real reactors. The interest of the WINCON programme [8] (WINfrith CONtainment) was at once to understand the influence of the presence of every internal structure in the global response of the reactor and to validate the codes SEUBNUK and EURDYN.

Based on a 1/30 scale model of the Superphenix reactor, the French programme MARA involved ten tests of gradual complexity due to the addition of internal deformable structures:
- MARA 1 and 2 [9] considered a vessel partially filled with water and closed by a rigid roof,
- MARA 4 [10] represented the main core support structures,
- MARA 8 and 9 [11] were closed by a flexible roof,
- MARA 10 [12] included the core support structures and a simplified representation of the above core structure (ACS).

The SIRIUS french code [13,14] was validated on the MARA programme [15,16]. As other codes using a Lagrangian approach, SIRIUS needed rezonings during calculation because the internal structure presence caused high distortion of the fluid meshes. Finite differences were used for the sodium and the roof and finite elements for the thin vessel. As the argon and the bubble were not meshed, a law related volume to pressure.

At the end of the 80s, it was preferred to add a specific HCDA sodium-bubble-argon tri-component constitutive law [17] to the general ALE fast dynamics finite element CASTEM-PLEXUS code. The HCDA constitutive law was qualified [18] on the CONT benchmark [19].

In order to demonstrate the CASTEM-PLEXUS capability to predict the behaviour of real reactors, axisymmetrical computations [20,21] of the MARA series were confronted with the experimental results. The computations performed at the beginning of the 90s showed a rather good agreement between the experimental and computed results for the MARA 8 test but it was concluded for the MARA 10 test that the discrepancies should be eliminated by increasing the fineness of the mesh [22].

As the method used for dealing with the fluid-structure coupling was improved since then, it was undertaken another comparison between the experimental and numerical results and a more detailed analysis of the results. After a brief presentation of the test-facility MARA 8 and of the code CASTEM-PLEXUS, this paper is focused on the numerical model and the analysis of the results computed by the code CASTEM-PLEXUS.

## 2 DESCRIPTION OF THE MARA8 TEST-FACILITY

The MARA8 experiment belongs to the MARA test programme defined and realised at the CEA-Cadarache in order to simulate a HCDA in small scale (1/30) mock-ups of the Superphenix reactor block. The characteristics of the mock-up were [22]:
- a scale factor of 1/30 for all dimensions and thickness,
- an axisymmetrical geometry,
- sodium was represented by water, argon by air and the bubble expansion by an explosive source.

All tests of the MARA series were fired using a 45 g low density low pressure explosive charge of L54/16 composition [23] leading at least to a 1000 MJ full scale energy release [16]. The bare vessels were filled with water leaving a 4.3 cm air gap [11]. All the vessels were identical and made of 316 steel of 1.2 mm thickness, except between the junctions with the core support plate and the internal heat exchangers where the thickness was locally reduced from 0.9 to 1.1 mm in order to simulate a pinned attachment with the diagrid.

In MARA8, a flexible roof of 10 mm thickness A42 steel was clamped to the roof support [11]. The vessel was welded to a flange bolted to the roof support. The MARA8 test-facility (Fig. 1) did not include internal structures. The explosive charge was hung from the roof centre.

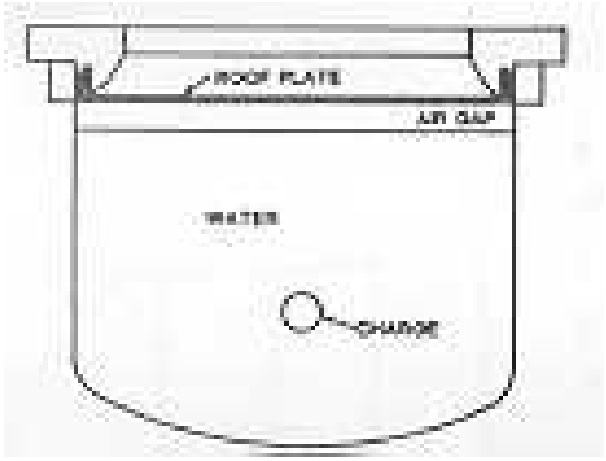


Fig. 1: The MARA8 test-facility

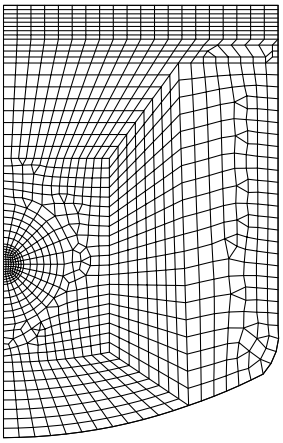

Fig. 2: Mesh of the MARA8 test

# 3 DESCRIPTION OF THE CASTEM-PLEXUS COMPUTER CODE AND OF THE HCDA CONSTITUTIVE LAW

CASTEM-PLEXUS [24,25,26] is a French general computer code, developed by the CEA-Saclay, for the analysis of fast transient phenomena. It can perform 1D, 2D or 3D structure calculations according to the problem to solve. The main fields dealt with are impacts [27], explosions [28,29], pipe circuits [30,31, 32, 33, 34, 35], hydrodynamics [36] and robots [37].

CASTEM-PLEXUS uses the Finite Element Method. The time integration is explicit and the formulation can be Lagrangian, Eulerian or ALE. The code can take into account various non-linearities related to the material or the geometry. CASTEM-PLEXUS solves successively, at each time step, the mass conservation, eventually the total energy equation if needed, the material constitutive law and finally the momentum conservation law.

For the purpose of simplifying the numerical model, we consider that, in the HCDA law, the sodium-argon-bubble mixture is homogeneous in each mesh and that the presence of the other components does not infer on the constitutive law of each one. We also assume that there is no thermal transfers between the components during the explosion. Owing to the last simplification, the code does not use the energy equation for the resolution of HCDA problem.

The mass conservation is computed by balancing the flows crossing the mesh boundary during the time step. The code solves the weak formulation of the momentum equation:
Mass conservation $M^{(n+1)} = M^{(n)} + \Delta M^{(n \to n+1)}$
with

$$\Delta M^{(n \to n+1)} = - \int_{t^{(n)}}^{t^{(n+1)}} \oint_A \rho \, \vec{n}.\vec{v} \, dA \, dt + \int_{t^{(n)}}^{t^{(n+1)}} \int_V M_{ext} \, dV \, dt$$

Weak formulation of the momentum conservation

$$\underbrace{\int_{t^{(n)}}^{t^{(n+1)}} \int_V \vec{\mathcal{U}}^* . \rho \frac{\partial \vec{v}}{\partial t} dV\, dt}_{M^{(n+1)}\,\gamma^{(n+1)}} + \underbrace{\int_{t^{(n)}}^{t^{(n+1)}} \int_V \vec{\mathcal{U}}^* . \left(\rho\, \vec{v} . \overline{\overline{\dot{\epsilon}}}\right) dV\, dt}_{\text{transport force}} - \underbrace{\int_{t^{(n)}}^{t^{(n+1)}} \oint_A \vec{n} . \left(\vec{\mathcal{U}}^* . \overline{\overline{\sigma}}\right) dA\, dt}_{\text{boundary conditions}}$$
$$+ \underbrace{\int_{t^{(n)}}^{t^{(n+1)}} \int_V \overline{\overline{\epsilon}}^* : \overline{\overline{\sigma}}\, dV\, dt}_{\text{internal forces}} = \underbrace{\int_{t^{(n)}}^{t^{(n+1)}} \int_V \vec{F}_{ext}\, dV\, dt}_{\text{external forces}}$$

with

| | | | |
|---|---|---|---|
| $A$ | surface | $V$ | volume |
| $\vec{F}_{ext}$ | external forces | $\vec{\gamma}$ | acceleration |
| $M$ | mass | $\rho$ | density |
| $M_{ext}$ | external mass source | $\vec{v}$ | velocity |
| $\vec{n}$ | normal vector | $\overline{\overline{\epsilon}}^*$ | strain (spatial derivative of $\vec{\mathcal{U}}^*$) |
| $n$ | time step | $\overline{\overline{\dot{\epsilon}}}$ | strain speed (spatial derivative of $\vec{v}$) |
| $t$ | time | $\overline{\overline{\sigma}}$ | stress |
| $\vec{\mathcal{U}}^*$ | arbitrary displacement | | |

In the finite element model, the nodal variables are the same for all the components (velocity, acceleration,). The elementary variables (pressure, density,) depend on several parameters : the partial variables of each component, the component presence fractions $x$... Let indicate with a subscript the quantities related to each constituent ($a$ for argon, $b$ for bubble, $s$ for sodium and $v$ for sodium vapour). Quantities without subscript are related to homogeneous mixture and index $g$ is related to gas mixture.

For instance, the mixture density is obtained by:

$$\rho = \rho_a\, x_a + \rho_b\, x_b + \rho_s\, x_s + \rho_v\, x_v$$

The mixture pressure $p_g$ is the sum of partial pressures:

$$p_g^{(n+1)} = p_a^{(n+1)} + p_b^{(n+1)} + p_v^{(n+1)} \qquad [1]$$

The void fraction $\alpha$ is obtained from the ratios between the relative density $\phi$ of a component (density related to the total volume of the mesh) and the absolute density of the component:

$$\alpha = \frac{\phi_a}{\rho_a} = \frac{\phi_b}{\rho_b} = \frac{\phi_v}{\rho_v} = \frac{\phi_g}{\rho_g} = 1 - \frac{\phi_s}{\rho_s} \qquad [2]$$

The fluid mixture is described by the constitutive laws of each component [20].

• Argon is assumed to be a perfect gas with an adiabatic behaviour:

$$p_a^{(n+1)} = p_a^{(n)} \left(\frac{\rho_a^{(n+1)}}{\rho_a^{(n)}}\right)^{\lambda_a} \qquad [3]$$

where $\lambda_a$ is the heat capacity ratio $c_p/c_v$ .

• The bubble is considered as a perfect gas whose behaviour follows a polytropic law:

$$p_b^{(n+1)} = p_b^{(n)} \left(\frac{\rho_b^{(n+1)}}{\rho_b^{(n)}}\right)^{\eta_b} \qquad [4]$$

The exponent $\eta_b$ can have any positive value. For instance, $\eta_b = 1$ for an isothermal law or $\eta_b = \lambda_b$ for an adiabatic law.

• Sodium is supposed to exist in a liquid phase and a gaseous shape because of the possibility of

cavitation. The diphasic sodium is supposed at saturation conditions and its temperature is assumed to be constant. The liquid is submitted to the pressure:

$$p_s^{(n+1)} = p_g^{(n+1)} = p_s^{(n)} + C_s^2 \left( \rho_s^{(n+1)} - \rho_s^{(n)} \right) \qquad [5]$$

with $C_s$ the sound velocity in sodium. The vapour only depends on the initial temperature $T^{(0)}$:

$$p_v^{(n+1)} = p_{sat} \left( T^{(0)} \right)$$

CASTEM-PLEXUS computes the average density and the concentration of each constituent from the mass conservation for each fraction. Then the pressure of the mixture is obtained by successive iterations. The iterative process computes:
1. the sodium density from [5] by estimating approximately $p_s^{(n+1)}$ at the beginning of the time step,
2. the void fraction and then the argon and bubble densities from [2],
3. the argon pressure from [3],
4. the bubble pressure from [4],
5. the pressure mixture from [1].

# 4 NUMERICAL MODELING OF THE TEST-FACILITY

The MARA8 test-facility is composed of structures and fluids interacting with each other. The mock-up is surrounded by a flexible roof and a flexible vessel. The structures are assumed to be thin and flexible enough to be represented by shells.

In case of HCDA, the internal fluids are sodium, argon and a gas bubble. In the test, these fluids were respectively replaced by water, air and an explosive charge. Water and air were initially at the atmospheric pressure whereas the explosive charge induced an initial pressure of 165 MPa in the bubble area. The characteristics taken into the numerical model are:

- Water : $\rho = 998.3$ kg/m3 sound speed $C = 1550$ m/s $p^{(0)} = 10^5$ Pa
- Air : $\rho = 1.206$ kg/m3 $\lambda = c_p/c_v = 1.4$ $p^{(0)} = 10^5$ Pa
- Explosive charge : $\rho = 400$ kg/m3 polytropic coef. $\eta = \lambda = 1.24$ $p^{(0)} = 1.646\,10^8$ Pa

Two kinds of fluid-structure coupling are available in the CASTEM-PLEXUS code. Their main differences lie in the definition of the local normal vector used to write the coupling relations between the freedom degrees of the fluid and the solid. The first fluid-structure coupling (FS2D instruction) requires the definition of coupling elements by the user and imposes to the fluid nodes to have the same displacements as the structure nodes. Besides, there is no automatic actualisation of the ALE grid for the elements other than the ones on the coupled lines. The second coupling (FSA instruction) goes without coupling elements; the code considers directly the fluid and solid nodes in contact and writes relations allowing a possible tangential movement of the fluid in relation to the structure. The FSA coupling is well adapted to complex geometries but it often implies a user intervention to pilot the displacements of the fluid ALE grid.

For the MARA8 test, the FS2D coupling was adopted because the geometry was sufficiently simple to define coupling elements easily and no huge distortion of the fluid mesh was waited. Owing to the symmetry of the mock-up, an axisymmetric representation (Fig. 2) was used for the numerical simulation.

The boundary conditions are:
- No horizontal displacement on the symmetry axis,
- No rotation of the two vessel and roof nodes located on the symmetry axis,
- Complete blocking of the node in the top corner at the junction between the vessel and the roof.

# 5 RESULTS

The interpretation of the numerical results is based on the analysis of the pressure, gas fraction, fluid speed, radial and vertical displacements, stresses and strains versus time. These variables are presented on drawings describing the state of the internal fluids or the structures at different instants.

## 5.1 Pressure

The pressure is presented on figure 3. Initially, the fluid inside the reactor is at the atmospheric pressure, except in the centre where is located the explosive charge simulating the high pressure bubble. The initial pressure of this zone is 165 MPa. This pressurised zone expands diametrally, thus creating the propagation of a pressure wave. Due to the expansion, the average pressure decreases conversely proportionally to the volume increase of the pressurised zone. After 0.1 ms, the pressure of the pressurised zone has fallen to 30 MPa.

The pressure wave contacts first the vessel bottom at 0.14 ms. Then the pressurised zone continues its expansion laterally by following the vessel shape. Simultaneously, a low pressure zone creates between the vessel bottom and the pressurised zone. The low pressure zone appears first next to the symmetry axis. The value of this low pressure zone is approximately the atmospheric pressure.

The pressure wave contacts the lateral part of the vessel at 0.22 ms. At that time, the pressure is around 20 MPa near the vessel and only 7 MPa in the initial pressurised zone in the middle of the mock-up. Because of the presence of the air layer below the roof, the overpressure is absorbed on the top by compression of the gas. This air blanket prevents from wave reflections on the top of the mock-up. The pressure wave coming from the centre, continues impacting the vessel laterally until approximately 0.35 ms. After that time, the pressure is less than 5 MPa in the whole fluid.

## 5.2 Gas fraction

The figure 4 presents the general volumic presence fraction of gas. In order to interpret correctly the presence of each component, the massic presence fractions of the bubble and air are described on figures 5 and 6. At the beginning, the gas presence is located in the middle at the bubble location and below the roof in the air blanket. Since 0.02 ms, a diphasic layer appears around the bubble: it is caused by the vaporisation of liquid water. The diphasic layer increases diametrally. During all the expansion phase of the pressure wave, the water remains saturated because of the local high pressure limiting the vaporisation. After 0.3 ms, the centre of the mock-up depressurises, what allows the presence of a fully vaporised zone next to the initial explosive charge.

The steam zone continues expanding with a spherical shape until about 4 ms. After this time, the steam near the vessel bottom starts condensing because the shell presence causes a pressure increase. Then the diphasic zone collapses little by little.

The air layer keeps its initial shape until 0.2 ms. At 0.3 ms, the air begins to be compressed near the symmetry axis and we can observe the presence of water in the bottom of the initial air layer. Progressively, the air is compressed and pushed in the top external corner. At 4.4 ms, the air zone has a minimum size and then it gets bigger.

## 5.3 The fluid velocity

The figures 7 and 8 show the fluid velocity by means of vectors indicating the flow direction and with a colour map. Initially, all the fluids are at rest. From 0.02 ms, the explosion expels violently the fluids out of the explosive charge zone and out of the periphery of the explosive zone. The fluid velocity is very high: around 200 m/s. Until 0.1 ms, the fluid moves with a uniform radial velocity.

From 0.1 to 0.4 ms, the explosive gas and water continue to expand radially at a speed decreasing from 150 m/s at the centre of the mock-up to 40 m/s near the vessel. The velocity is no more uniform: we observe vertical speeds up to 200 m/s on the symmetry axis. This artefact is probably caused by the presence of the boundary conditions on the axis. In the air zone, the velocities are oriented upwards and remain limited to 40 m/s.

From 0.6 to 1.4 ms, we note the same radial expansion in the centre. The fluid near the lateral wall of the vessel starts flowing upwards slowly. The fluid trapped in the bottom corner tries to evacuate by the bottom following the vessel shape towards the central axis. On the top of the mock-up, the air is pushed horizontally towards the external top corner joining the vessel to the roof.

Until 3 ms, we observe several fluid orientation changes. The water in the centre starts moving upwards. In the lower part of the mock-up, we can note the presence of contradictory flow directions in neighbouring elements. The speeds are less than 20 m/s in the bottom of the mock-up. However, the speeds remain high (up to 60 m/s) in the upper part of the mock-up. Near the roof, the air is still pushed in the top corner while water flows upwards near the symmetry axis and tries to move away from the lateral wall. In the top corner, the air speed reaches locally 200 m/s.

Between 3 and 5 ms, we observe high speeds (up to 150 m/s). They are due to a general rebound of the fluid against the vessel. The water of the bottom and of the bottom corner comes back again to the central part of the mock-up. The rest of water continues flowing upwards, except water near the air layer. In that area, the water located near the vessel tries to flow outwards and the one located at half vessel radius returns towards the symmetry axis. Globally, the velocities near the vessel are much lower than in the centre. The air in the top corner is expelled horizontally along the roof and downwards along the vessel.

Later, the water globally comes back to the mock-up centre. Near the vessel, it slows down. The air in the top corner is pushed back along the roof at high speed.

### 5.4 Deformed shape

The deformed shape of the mesh is presented on figure 9. The vessel deforms first at the bottom: at 0.4 ms, we observe a going down of the vessel bottom due to the pressure wave impact. This deformation increases until the end of the computation and represents the most important vessel displacement. Between 0.4 and 2 ms, the vessel deforms radially. A large bulge appears approximately half-way up the mock-up height. It is caused by the impact of the water expelled from the mock-up centre and which arrives perpendicularly to the vessel

The centre of the roof starts deforming from 2 ms. Progressively, the whole roof is lifted starting from the centre. The deformation is maximum on the symmetry axis and decreases when one goes away towards the external radius. This bulge is due to the impact of the water coming from the central part of the mock-up; the water changed direction after the impact against the lateral wall of the vessel and went up.

From 3.8 ms, a vessel bulge appears in the upper part of the vessel near the junction with the roof. The deformation is concentrated in a small area but its amplitude is more important than the one of the previous lateral bulge. It is due to the compression of air in the top external corner.

One can remark that the grid deformation is concentrated in the elements on the edge of the coupled fluid-structure lines.

### 5.5 Radial displacements of the structures

The figure 10 shows the radial structure displacements. The first displacement appears at the bottom of the lateral wall of the vessel, just above the bottom corner: it is of about 5 mm at 0.6 ms. Then the radial displacement increases a bit higher up and the deformed zone extends. The maximum

displacement reaches 15 mm since 2.2 ms. This displacement corresponds to the constitution of the lower bulge in the lateral wall.

A radial displacement appears on the vessel bottom at half radius from 1.6 ms. Between 2.2 ms and the end of the computation, this displacement remains stable. The local maximum value is 7 mm. This displacement comes from the lowering of the vessel bottom.

A third radial displacement occurs in the upper part of the lateral wall of the vessel from 3.6 ms. Progressively, the deformed area extends and the displacement increases. The maximum value is 20 mm and is reached since 5 ms. This displacement is due to the late creation of the upper bulge in the lateral wall.

No radial displacement happens in the roof because of the modeling, the node in the external top corner being completely locked.

### 5.6 Vertical displacements of the structures

The vertical displacements are shown on figure 11. A downwards displacement is observed on the vessel bottom during the whole computation. It starts near the symmetry axis and extends progressively to the rest of the lower part of the vessel until the bottom corner. The maximum value is 55 mm at the end of the computation (7 ms). This displacement corresponds to the downwards deformation of the vessel bottom.

From 2.6 ms, an upwards displacement happens in the roof. It starts at the centre of the roof and extends towards the roof edge. The maximum displacement is 30 mm; it is located on the symmetry axis. This upwards displacement is due to the roof lift under the upward directed water thrust.

Between 1.4 and 3.2 ms, the lower part of the lateral wall of the vessel moves down. It is pulled by the going down of the vessel bottom and also pushed down by the water expelled from the mock-up centre and impacting the vessel with an incident angle oriented downward. The downward displacement remains limited to 5 mm.

At 3.8 ms, the lateral wall takes again its initial location: it is in equilibrium between the downward thrust on the vessel bottom and the upward thrust on the roof. Since 4.6 ms, the upper part of the lateral wall and then the complete lateral wall are pulled upward. This displacement probably comes from the upward fluid flow against the wall. It cannot be caused by the roof lift owing to the complete blocking of the point in the outer top corner. The displacement value remains limited to 5 mm.

### 5.7 Von Mises stresses in the structures

The figure 12 shows the stresses. Stresses occur first in the vessel bottom, near the symmetry axis. These stresses are due to the arrival of the pressure wave hitting the vessel bottom at that time and to the pressure wave propagation along the vessel. The stress value reaches very soon 500 MPa near the axis and remain constant at that location until 0.32 ms. Between 0.2 and 0.26 ms, the area under stress extends to the whole vessel bottom. We observe the presence of three spots of very high stresses near the bottom corner. They correspond to the junctions between the vessel parts of reduced thickness and the rest of the vessel.

Between 0.32 ms and 0.4 ms, the stresses decrease slightly in the vessel bottom but concentrate in the bottom corner. Until 2.4 ms, the stresses increase again and reach an average value of 500 MPa in the whole vessel bottom. Simultaneously, the stresses increase in the lateral part of the vessel but their value remains more limited: between 200 and 300 MPa. This stress increase corresponds to the shock and splashing of water against the wall.

After 3 ms, the stresses reduce progressively in the whole vessel, except in the top corner where a plastic hinge is created. This decrease is linked to the rebound of water on the shell followed by a flow direction change towards the centre and the top of the mock-up. On the contrary, the stresses start increasing in the roof from that time. Nevertheless, they remain limited: less than 300 MPa.

### 5.8 Plastic strains in the structures

The figure 13 exhibits the plastic strains. No plasticity appears before 1.2 ms. Then plastic strains happen at the same time in the vessel bottom near the symmetry axis and half-way up the lateral wall of the vessel. They come from the deformations of the vessel bottom and the creation of the large bulge in the lower part of the lateral wall. Their level increase until about 3.6 ms. After that time, the plastic strains remain stable in those parts of the vessel. The maximum strains are 16 % at the centre of the vessel bottom and 6 % for the lower bulge in the lateral wall.

From 3.2 ms, plasticity happens in the upper part of the lateral wall. A plastic hinge is created in the top corner at the junction between the vessel and the roof: the plastic strain value reaches 10 % there. Plastic strains also appears at the location of the upper bulge in the lateral wall. The maximum value is 16 % and is located where the vessel displacement is maximum.

## 6 CONCLUSION

In this paper, we presented a computation of the MARA8 test simulating a HCDA. The test consists in an explosion in a steel vessel covered with a flexible roof. An explosive charge is placed in the middle of the test-facility. The vessel is filled with water, topped by an air blanket below the roof. A specific HCDA constitutive law was developed in the CASTEM-PLEXUS code to simulate this kind of explosion.

The code computed successfully the explosion during 7 ms of physical time. The computation shows the propagation of a pressure wave from the explosive zone towards the external structures. Water vaporises in the middle and the air layer is concentrated in the top corner of the test-facility. The vessel bottom and the roof move away and two bulges appear in the lateral wall of the vessel.

For testing the influence of the internal structures of the following tests of the MARA series (MARA10 and MARS tests), specific developments were undertaken in the CASTEM-PLEXUS code: the internal structures of complex geometry were represented by homogenizing the structures with the surrounding fluid [38,39].

## REFERENCES

[1] Cagliostro, D.J., Florence, A.L., Abrahamson, G.R., 1979. Scale modeling in LMFBR safety, Nuclear Engineering and Design 55, 235-247.
[2] Kendall, K.C., Adnams, D.J., 1986. Experiments to validate structural dynamics code used in fast reactor safety assessment, Science and Technology of Fast Reactor Safety, Vol. 2, British Nuclear Energy Society, London, England.
[3] Holtbecker, H., 1977. Testing philosophy and simulation techniques, Nuclear Engineering and Design 42, 75-87.
[4] Hoskin, N.E., Lancefield, M.J., 1978. The COVA programme for the validation of computer codes for fast reactor containment studies, Nuclear Engineering and Design 46, 17-46.
[5] Albertini, C., et al. The JRC-COVA programme : Final Report. Commission of the European Communities, Report EUR 8705, 1983. Nuclear Science and Technology, 1984, pp. 1-182.
[6] Wenger, H.U., Smith, B.L., 1987. On the origin of the discrepancies between theory and experiment in the COVA series, Proc. 9th Int. Conf. on Structural Mechanics In Reactor Technology, Vol. E, Lausanne, Switzerland, pp. 339-344.
[7] Kendall, K.C., Benuzzi, A., 1980. The COVA programme : Validation of the fast reactor containment code SEURBNUK, Nuclear Engineering and Design 57, 79-105.
[8] Sidoli, J.E.A., Kendall, K.C. The WINCON programme - Validation of the fast reactor primary containment codes. Proc. INE Int. Conf. On Nuclear Containment, Cambridge, England, April 1987. Nuclear Containment Structures, D.G. Walton, Cambridge University Press, 1988.

[9] Acker, D., Benuzzi, A., Yerkess, A., Louvet, J., August 1981. MARA 01/02 - Experimental validation of the SEURBNUK and SIRIUS containment codes, Proc. 6th Int. Conf. on Structural Mechanics In Reactor Technology, Section E3/6, Paris, France.
[10] Smith, B.L., Fiche, C., Louvet, J., Zucchini, A., August 1985. A code comparison exercise based on the LMFBR containment experiment MARA-04. Proc. 8th Int. Conf. on Structural Mechanics In Reactor Technology, Section E4/7, Brussels, Belgium, pp. 151-157.
[11] Fiche, C., Louvet, J., Smith, B.L., Zucchini, A., August 1985. Theoretical experimental study of flexible roof effects in an HCDA's simulation, Proc. of 8th Int. Conf. on Structural Integrity In Reactor Technology, Section E4/5, Brussels, Belgium, pp. 139-144.
[12] Louvet, J., Hamon, P., Smith, B.L., Zucchini, A., August 1987. MARA 10: an integral model experiment in support of LMFBR containment analysis, Proc. 9th Int. Conf. on Structural Mechanics In Reactor Integrity, Section E, Lausanne, Switzerland, pp. 331-337.
[13] Blanchet, Y., Obry, P., Louvet, J., August 1981. Treatment of fluid-structure interaction with the SIRIUS computer code, Proc. . 6th Int. Conf. on Structural Mechanics In Reactor Technology, Section B8/8, Paris, France.
[14] Daneri, A., Toselli, G., Trombetti, T., Blanchet, Y., Louvet, J., Obry, P, August 1981. Influence of the representation models of the stress-strain law on the LMFBR structures in an HCDA, Proc. of 6th Int. Conf. on Structural Integrity In Reactor Technology, Section E4/4, Paris, France.
[15] Bour, C., Spérandio, M., Louvet, J., Rieg, C., August 1989. LMFBR's core disruptive accident. Mechanical study of the reactor block, Proc. 10th Int. Conf. on Structural Mechanics In Reactor Technology, Vol. E, Anaheim, pp. 281-287.
[16] Louvet., J., August 1989. Containment response to a core energy release. Main experimental and theorical issues - Future trends, Proc. 10th Int. Conf. on Structural Mechanics In Reactor Integrity, Vol. E, Anaheim, pp. 305-310.
[17] Lepareux, M., Bung, H., Combescure, A., Aguilar, J., August 1991. Analysis of a CDA in a LMFBR with a multiphasic and multicomponent behaviour law, Proc. 11th Int. Conf. on Structural Mechanics In Reactor Integrity, Section E13/1, Tokyo, Japan, pp. 371-376.
[18] Casadei, F., Daneri, A., Toselli, G., August 1989. Use of PLEXUS as a LMFBR primary containment code for the CONT benchmark problem, Proc. of 10th Int. Conf. on Structural Mechanics In Reactor Technology, Section E13/1, Anaheim, pp. 299-304.
[19] Benuzzi, A., 1987. Comparison of different LMFBR primary containment codes applied to a benchmark problem, Nuclear Engineering and Design 100, 239-249.
[20] Lepareux, M., Bung, H., Combescure, A., Aguilar, J., Flobert, J.F., August 1993. Analysis of an HCDA in a fast reactor with a multiphase and multicomponent behavior law, Proc. 12th Int. Conf. on Structural Mechanics In Reactor Integrity, Section E7/2, Stuttgart, Germany, pp. 197-202.
[21] Cariou, Y., Pirus, J.P., Avallet, C., August 1997. LMR large accident analysis method, Proc. of 14th Int. Conf. on Structural Mechanics In Reactor Technology, Section P3/7, Lyon, France, pp. 395-402.
[22] Cariou, Y., Spérandio, M., Lepareux, M., Christodoulou, K., August 1993. LMFBR's whole core accident. Validation of the PLEXUS code by comparison with MARA tests, Proc. of 12th Int. Conf. on Structural Mechanics In Reactor Technology, Section E7/4, Stuttgart, Germany.
[23] David, F., 1978. Etude d'une composition explosive flegmatisée. Applications à la déformation d'une cuve, Proc. Symposium sur les hautes pressions dynamiques, Paris, France.
[24] Chavant, C., Hoffmann, A., Verpeaux, P., Dubois, J., 1979. Plexus: A general computer code for explicit Lagrangian computation, Proc. 5th Int. Conf. on Structural Integrity In Reactor Technology, Section B2/8, Berlin, Germany.
[25] Hoffmann, A., Lepareux, M., Schwab, B., Bung, H., 1984. Plexus - A general computer program for fast dynamic analysis, Proc. of the Conference on Structural Analysis and Design on Nuclear Power Plant, Porto Alegre, Brazil.

[26] Robbe, M.F., Lepareux, M., Bung, H. Plexus - Notice théorique, CEA report DMT/94-490, 1994.
[27] Robbe[a], M.F., Galon, P., Yuritzinn, T., November 1999. Castem-Plexus: Un logiciel de dynamique rapide pour évaluer l'intégrité des structures en cas d'accident, Proc. 4th Conf. INSTRUC, Courbevoie, France.
[28] Robbe, M.F., Lepareux, M., Vivien, N., Cénérino, G., August 1997. Screening calculations on the vessel lower head behaviour due to an in-vessel steam explosion, Proc. 14th Int. Conf. on Structural Mechanics In Reactor Technology, Section PW/9, Lyon, France.
[29] Robbe[a], M.F., Lepareux, M., April 2000. Scoping calculations of an in-vessel steam explosion. CASTEM-PLEXUS computations, Proc. 8th Int. Conf. On Nuclear Engineering, paper 8269, Baltimore, USA.
[30] Lepareux[a], M., Schwab, B., Hoffmann, A., Jamet, P., Bung, H., 1985. Un programme général pour l'analyse dynamique rapide - Cas des tuyauteries, Proc. Colloque Tendances Actuelles en Calcul des Structures, Bastia, France.
[31] Lepareux[b], M., Schwab, B., Bung, H., August 1985. Plexus A general computer program for the fast dynamic analysis The case of pipe-circuits, Proc. 8th Int. Conf. on Structural Mechanics In Reactor Integrity, Vol. F1 2/1, Brussels, Belgium.
[32] Robbe[b], M.F., Lepareux, M., Trollat, C., August 1999. Hydrodynamic loads on a PWR primary circuit due to a LOCA. Pipe computations with the CASTEM-PLEXUS code, Proc. 15th Int. Conf. on Structural Mechanics In Reactor Technology, Section J05/4, Seoul, Korea.
[33] Robbe[b], M.F., Potapov, S.V., April 2000. A pipe-model to assess the hydrodynamic effects of a blowdown in a 4-loop PWR, Proc. 8th Int. Conf. On Nuclear Engineering, paper 8156, Baltimore, USA.
[34] Robbe[c], M.F., Lepareux, M., Trollat, C., April 2000. Assessment of the hydrodynamic loads due to a LOCA in a 3-loop PWR. CASTEM-PLEXUS computations, Proc. 8th Int. Conf. On Nuclear Engineering, paper 8203, Baltimore, USA.
[35] Potapov, S.V., Robbe, M.F., Téphany, F., September 2000. Hydrodynamic consequences of a LOCA in a 4-loop PWR. Proc. European Congress on Computational Methods in Applied Sciences and Engineering (ECCOMAS), Barcelona, Spain.
[36] Struder, E., Galon, P., 1997. Hydrogen combustion loads Plexus calculations, Nuclear Engineering and Design 174, 119-134.
[37] Lepareux, M., Michelin, J.M., Thiault, D. Plexus-R : une extension de Plexus à la robotique, CEA report DMT/94-138, 1994.
[38] Robbe, M.F., August 1999. A porosity method to model the internal structures of a reactor vessel, Proc. 15th Int. Conf. on Structural Mechanics In Reactor Technology, Vol. B, Seoul, Korea.
[39] Robbe, M.F., Bliard, F., April 1999. A porosity model to represent the influence of structures on a fluid flow. Application to a hypothetical core disruptive accident, Proc. 7th Int. Conf. On Nuclear Engineering, paper 7819, Tokyo, Japan.

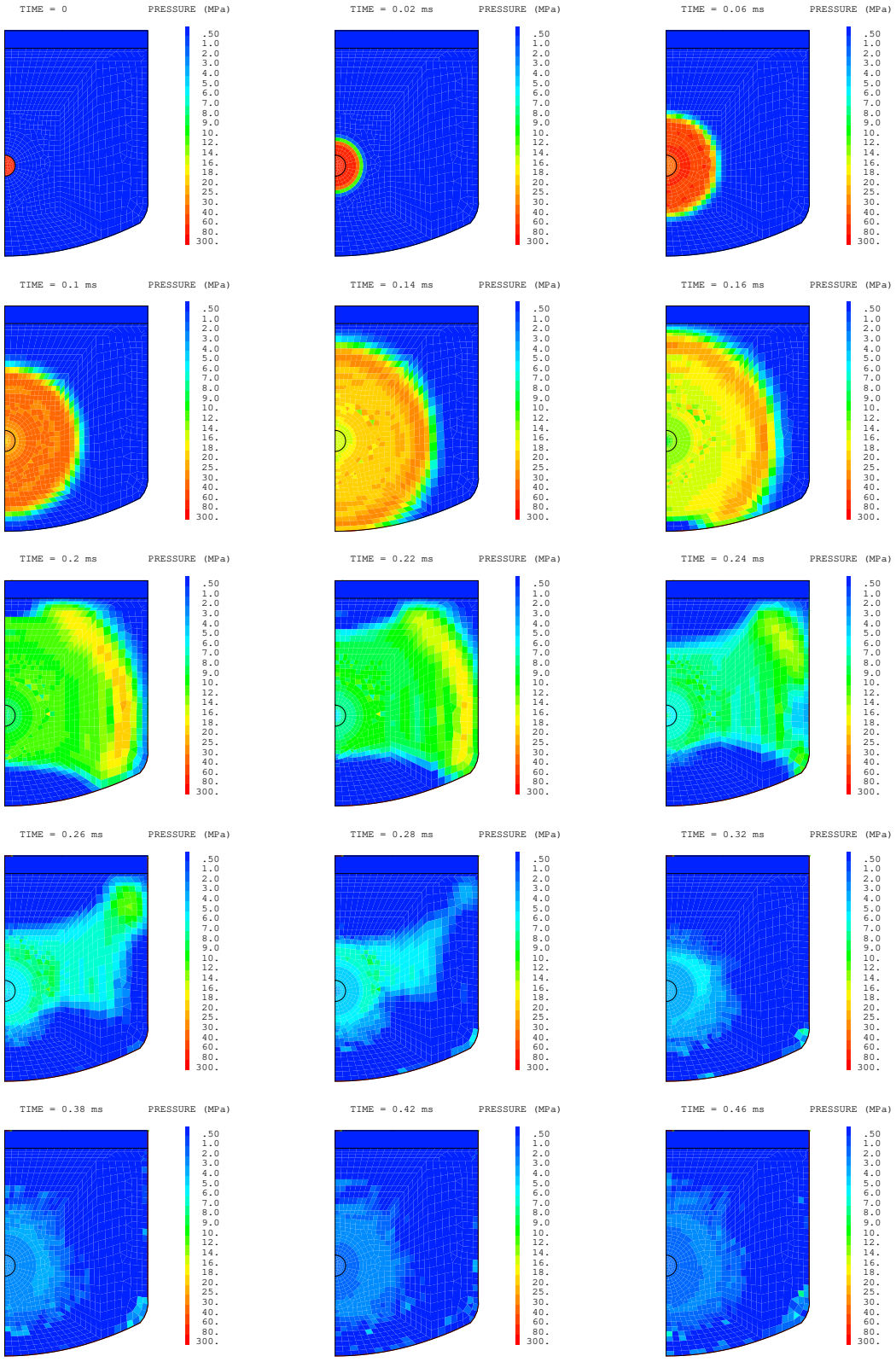


Fig. 3: Pressure computed for the MARA8 test

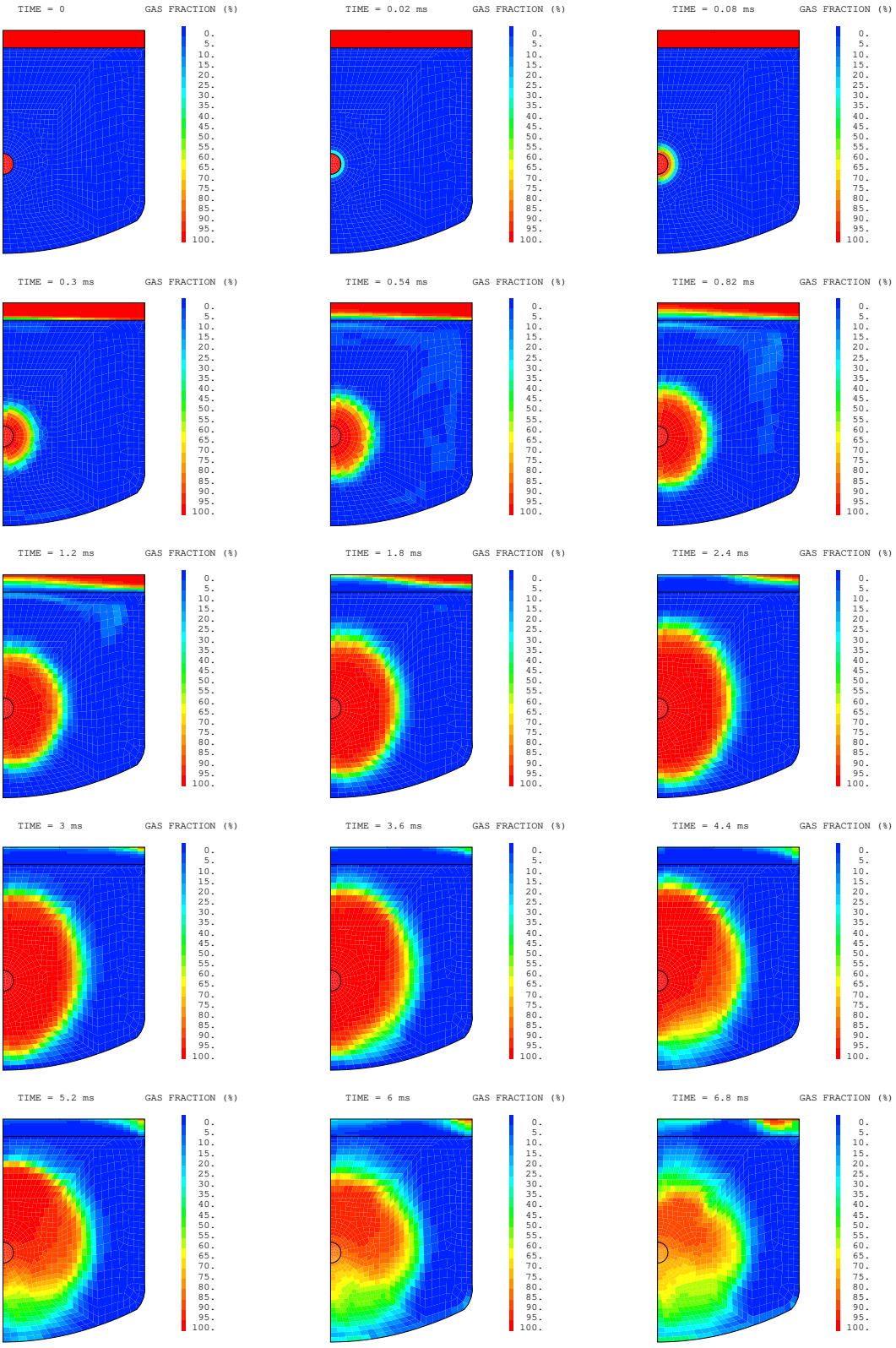


Fig. 4: Gas fraction computed for the MARA8 test

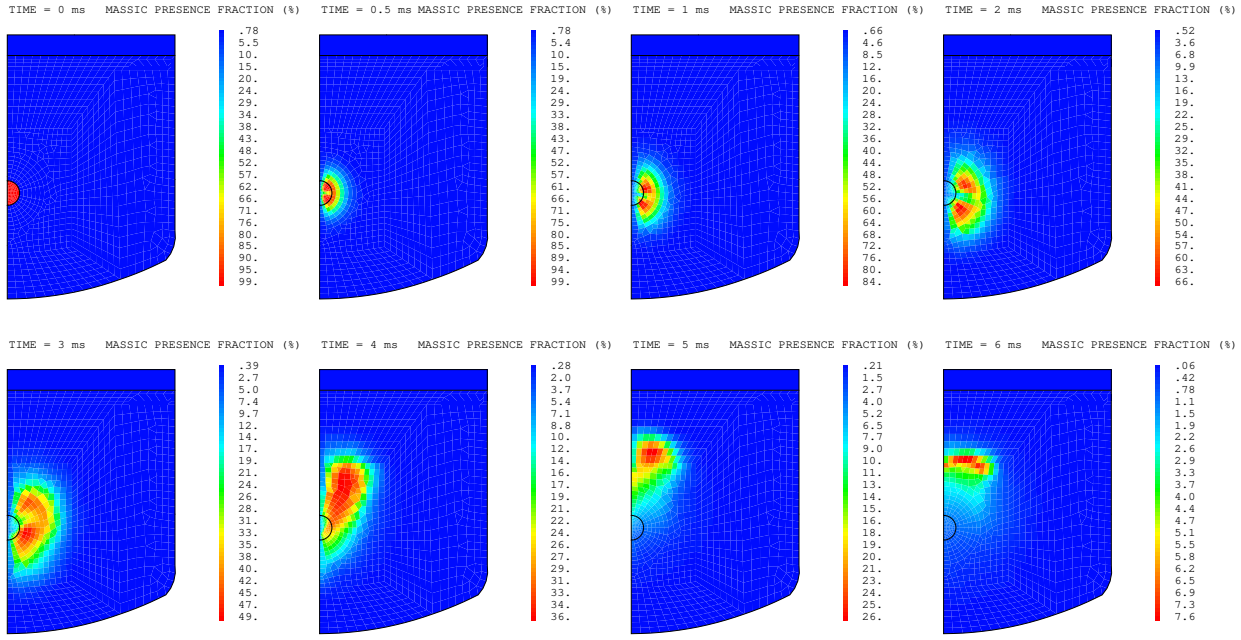


Fig. 5: Bubble massic presence fraction

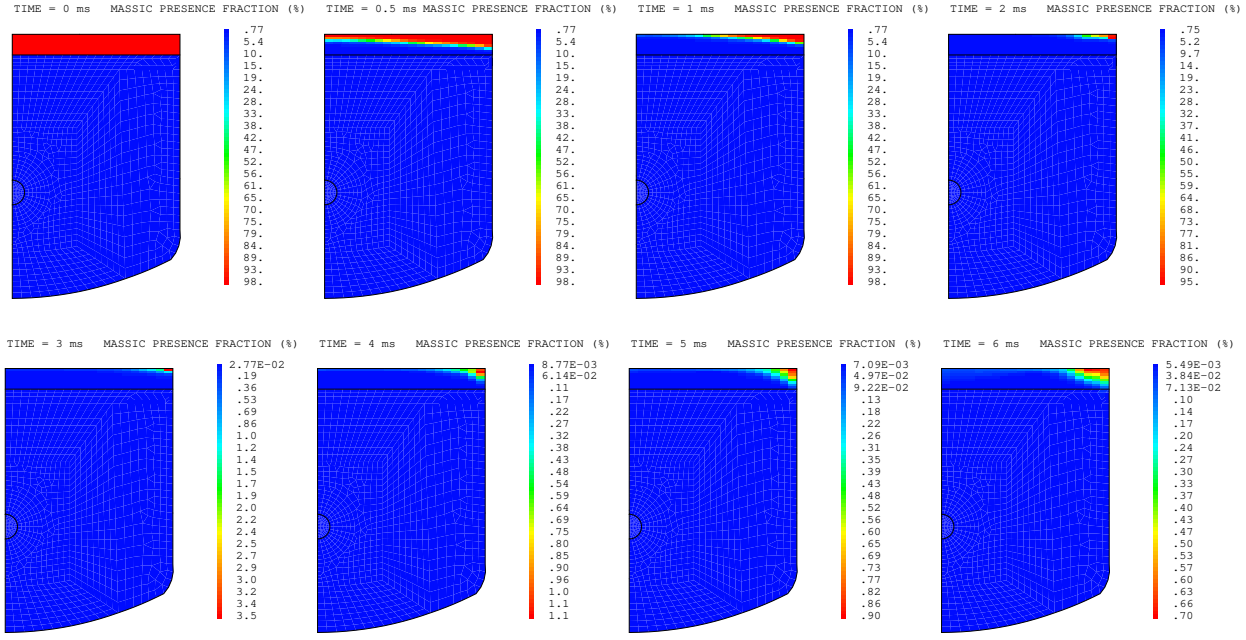


Fig. 6: Air massic presence fraction

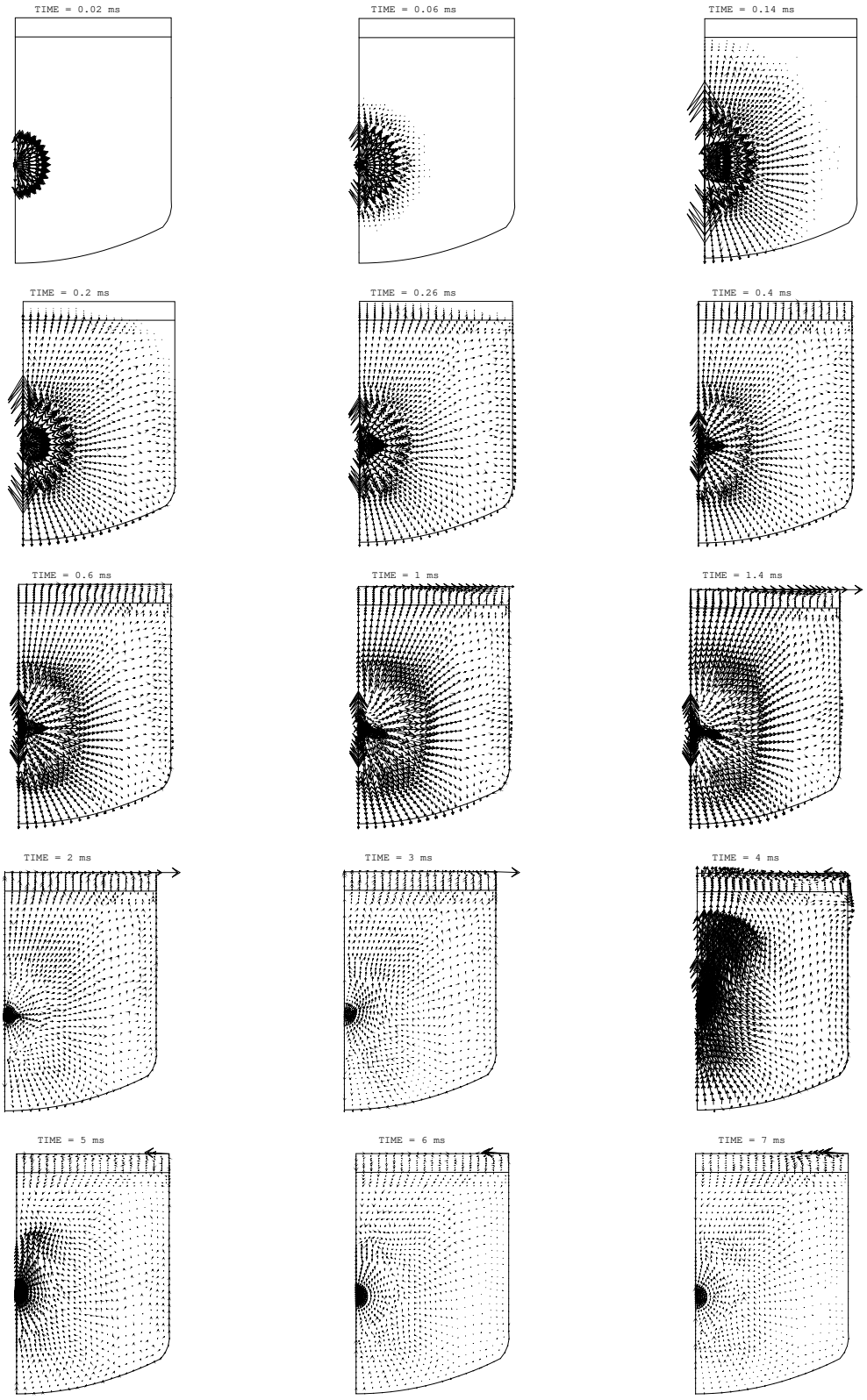


Fig. 7: Fluid speed computed for the MARA8 test

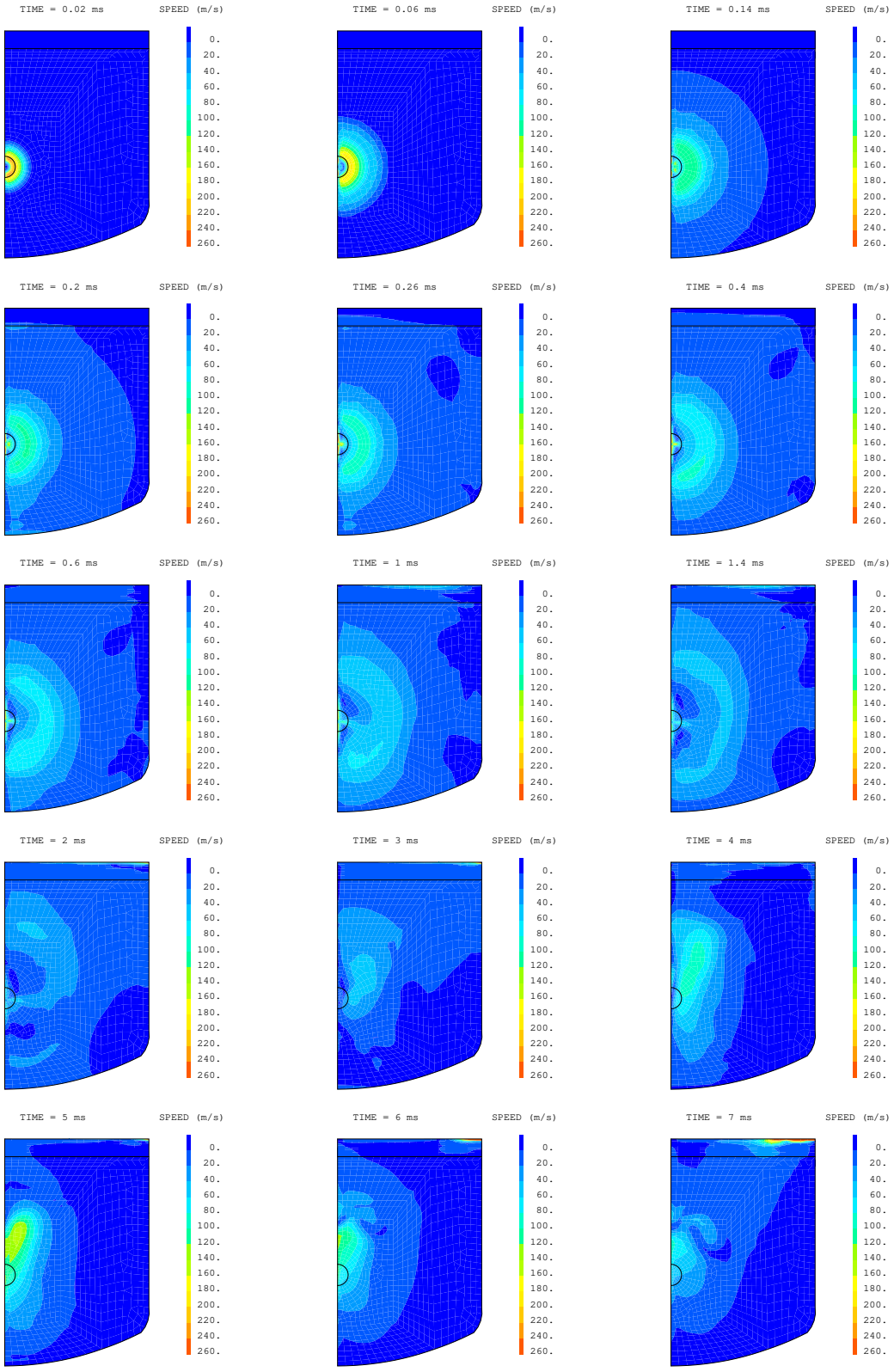


Fig. 8: Fluid speed computed for the MARA8 test

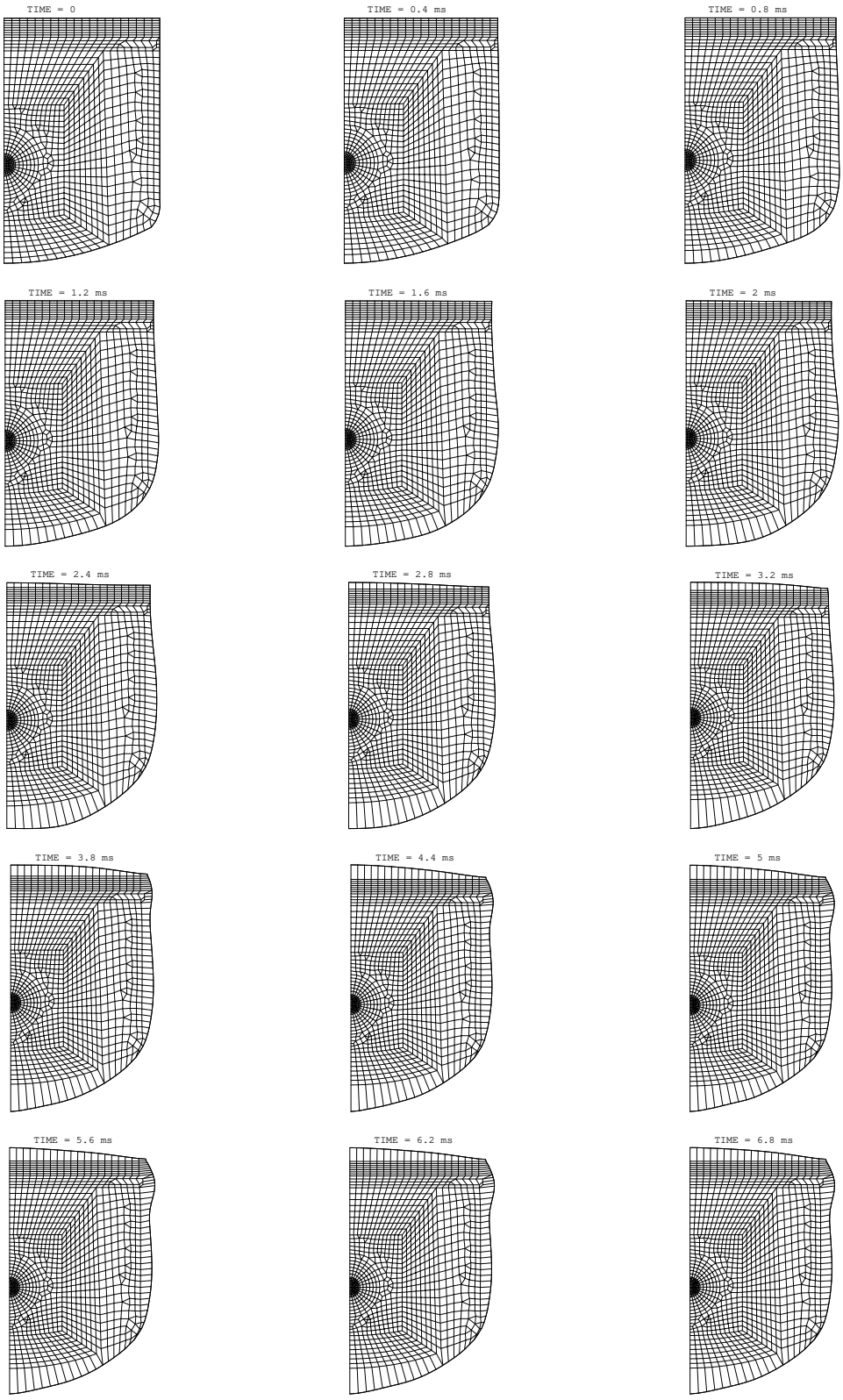


Fig. 9: Deformed shape for the MARA8 test

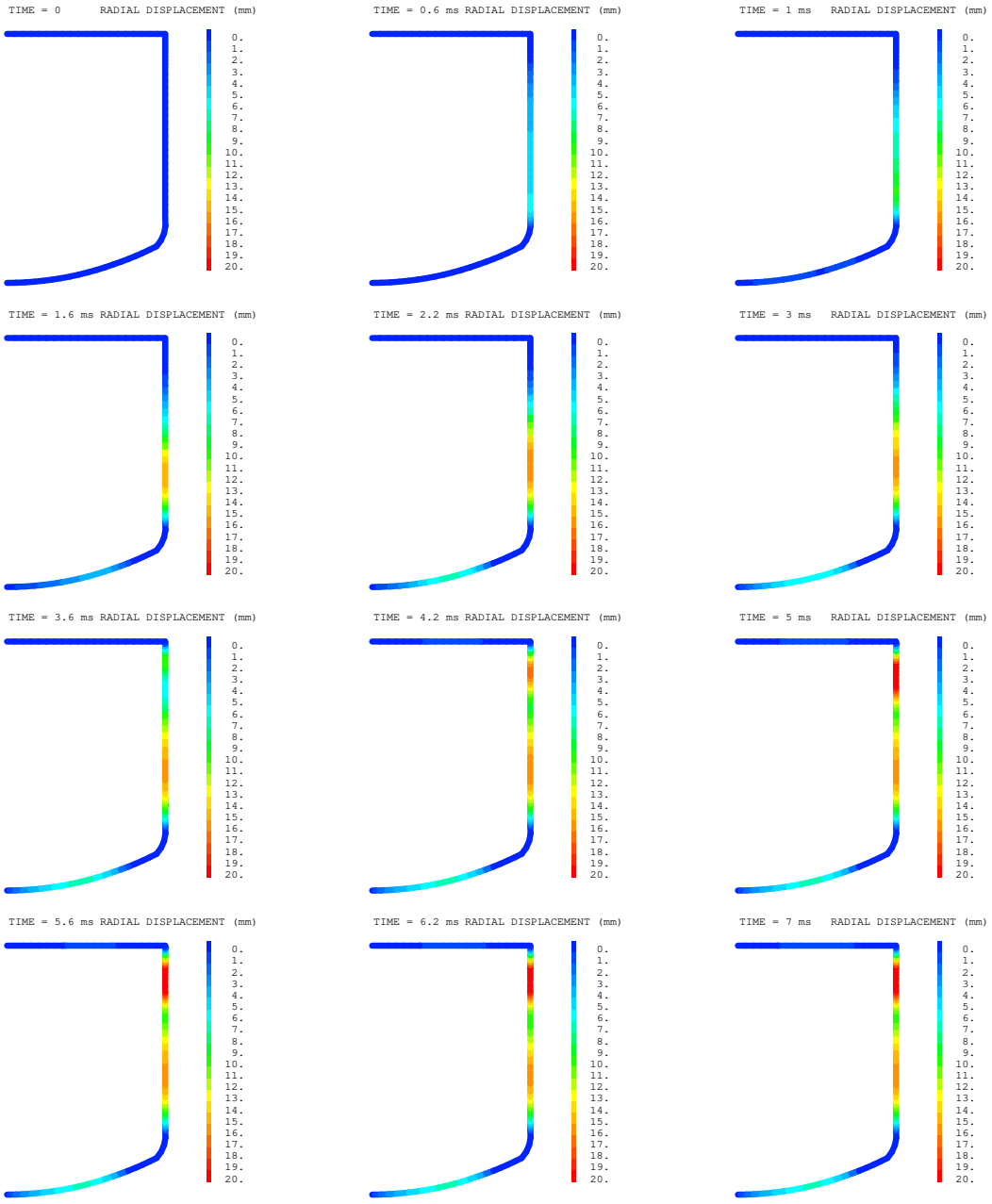


Fig. 10: Radial structure displacements for the MARA8 test

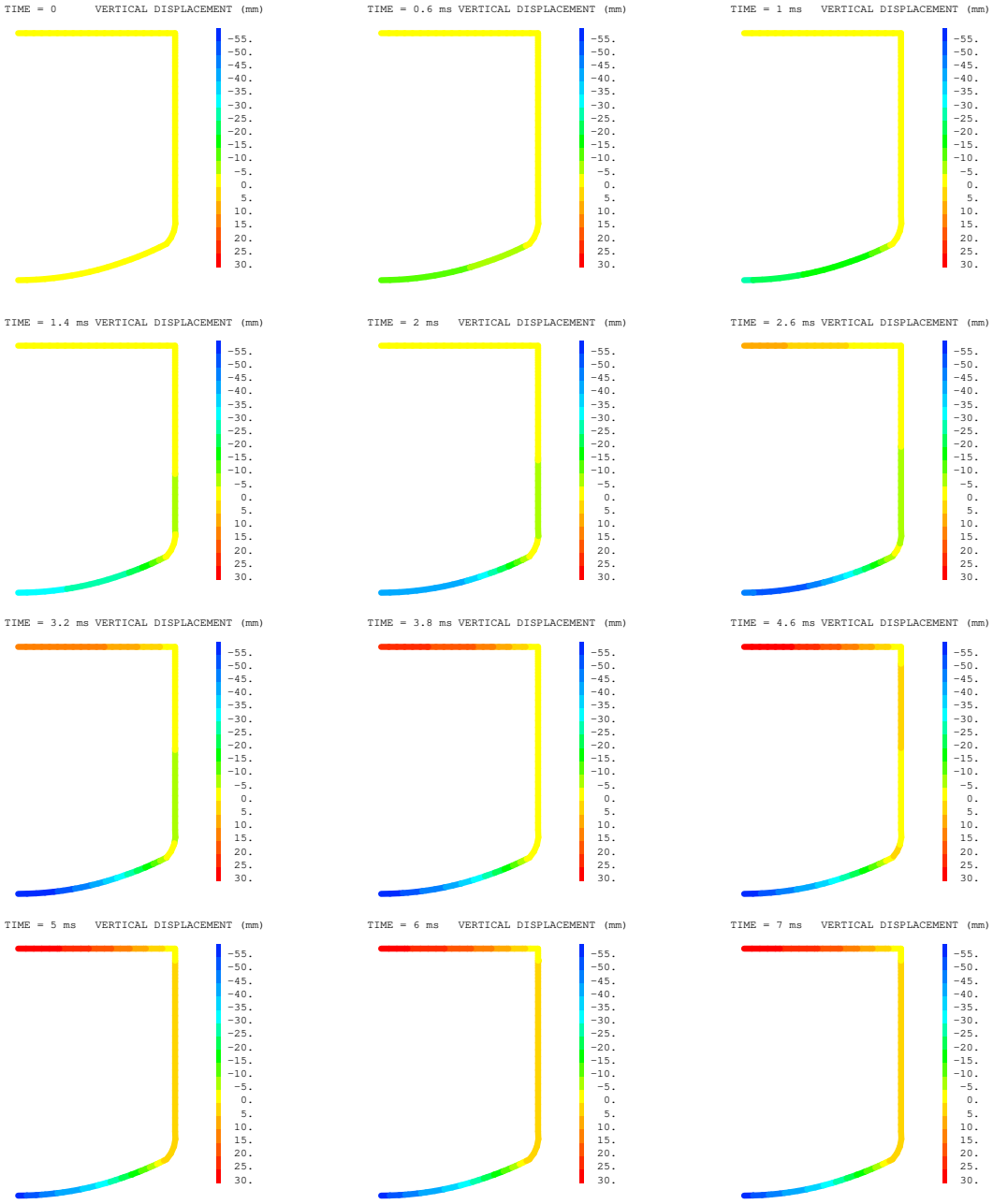


Fig. 11: Vertical structure displacements for the MARA8 test

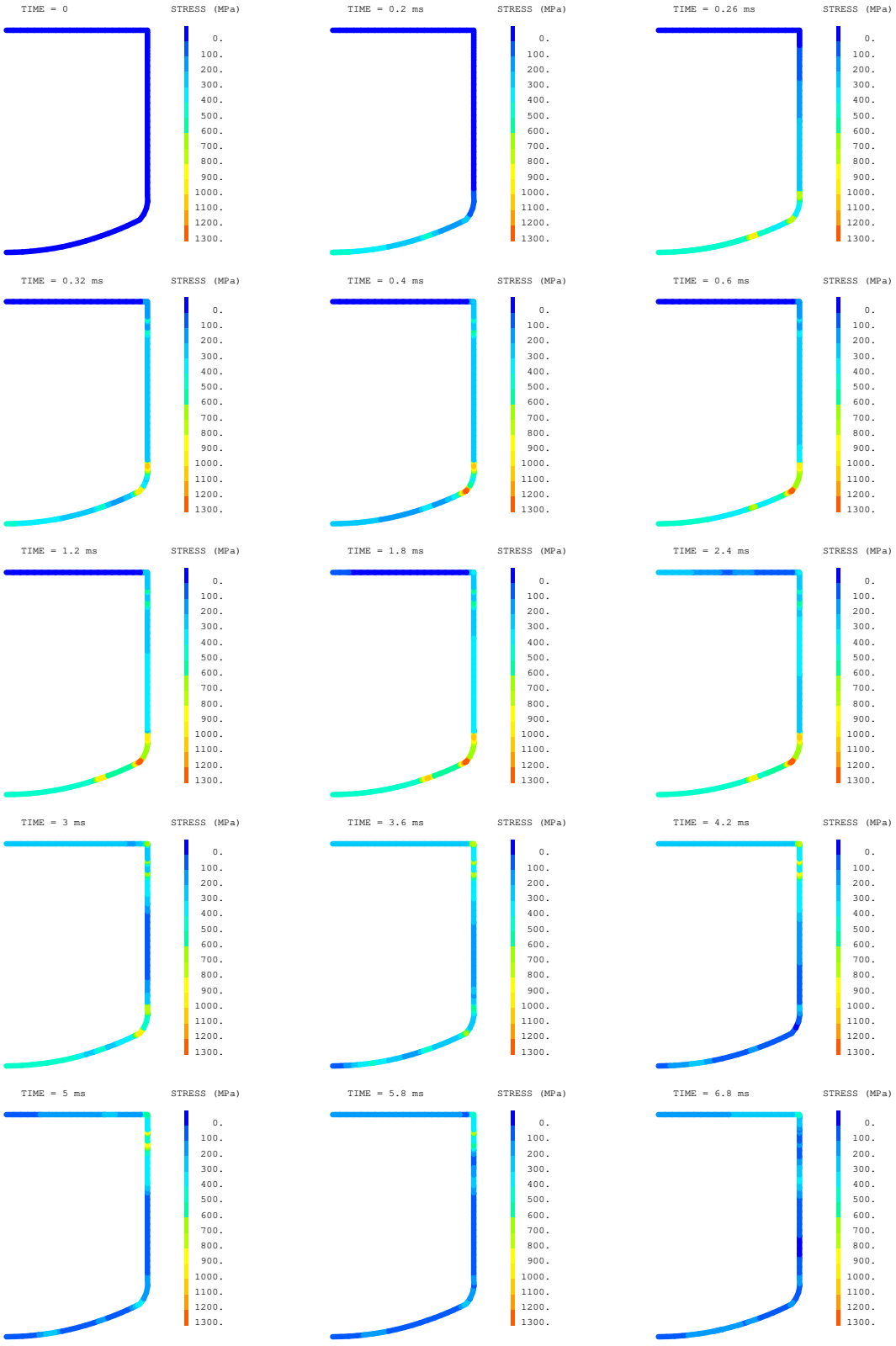


Fig. 12: Von Mises stresses for the MARA8 test

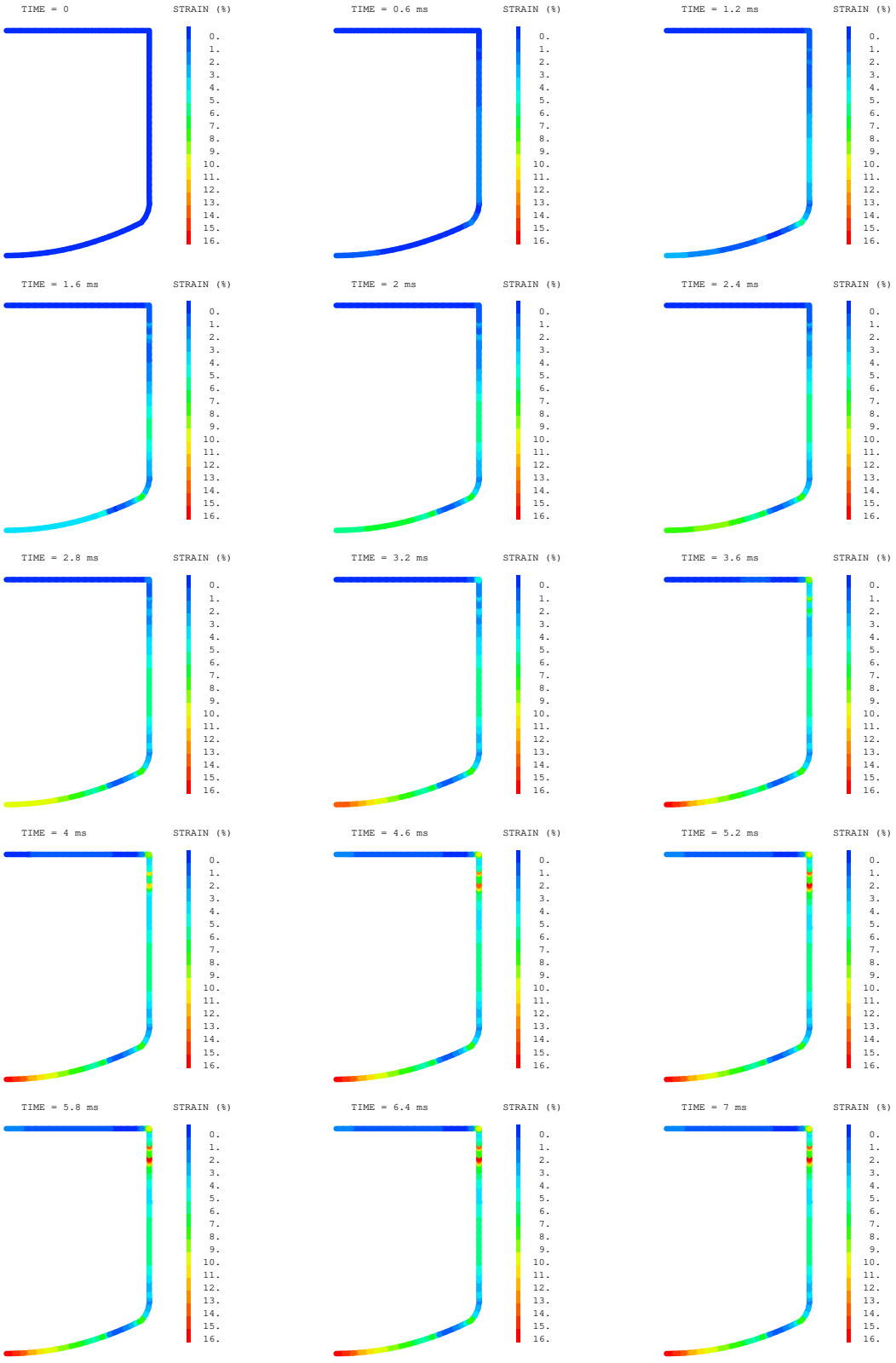


Fig. 13: Plastic strains for the MARA8 test